REVERBERATION CHAMBER AS A MULTIVARIATE PROCESS: FDTD EVALUATION OF CORRELATION MATRIX AND INDEPENDENT POSITIONS

G. Gradoni[1, *], V. Mariani Primiani[2], and F. Moglie[2]

[1]Institute for Research in Electronics and Applied Physics, University of Maryland, College Park, MD 20742, USA

[2]DII, Università Politecnica delle Marche, Via Brecce Bianche, 12, Ancona 60131, Italy

Abstract—This paper evaluates the mode-stirring efficiency in terms of uncorrelated positions of a mechanical stirrer operating inside a reverberation chamber (RC). The actual RC is simulated and viewed as a multivariate random process: the chamber field is sampled in a lattice of spatial points distributed uniformly over a volume of arbitrary dimensions. By adopting such a grid, the stirrer efficiency is then computed through the correlation matrix, accounting for the residual correlation between stirrer positions. The second-order statistics are calculated averaging over the sampling volume. Results are presented for two stirrers that move in both synchronous and interleaved mode. A comparison with the traditional circular correlation (CC) method, for the determination of the uncorrelated positions, is done showing how CC overestimates stirrer efficiency.

1. INTRODUCTION

Reverberation chambers (RC) are widely used in electromagnetic compatibility (EMC) to carry out immunity and emission tests [1]. Beside these traditional EMC applications, these electrically large cavities are also used for antenna testing [2, 3], to replicate multipath propagation in testing wireless devices [4–8], and also for the material scattering cross section determination [9]. The RC random field properties make them appealing also to study human exposure to electromagnetic field [10, 11]. In the last years the RC was used to measure the shielding effectiveness (SE) of enclosure [12–15], and

* Corresponding author: Gabriele Gradoni (ggradoni@umd.edu).

the shielding properties of materials [16, 17], using a nested RC [18]. Particular effort was devoted in studying RC field statistical properties in both ideal [19] and non ideal conditions [20, 21], also analyzing what happens approaching chamber boundaries [22]. The analysis of RC field can be accurately done by means of powerful numerical tools able to account for complex geometries such as those based on the FDTD technique [23–26], based on the application of the image theory to account for reflecting boundaries [27], based on the application of hybrid techniques [28], based on the plane-wave integral representation [29–32], and comparing more numerical techniques [33]. These analyses highlighted the importance of the mechanical blades in the stirring process, suggesting a deep investigation of the geometrical parameters that affect stirrer performance [34]. The use of multiple blade systems can enhance stirring efficiency but it depends on the way they are moved [35, 36], and new stirrer shapes that enhance its performance are obtained by FDTD simulations [37]. One of the main parameters used to check stirrer efficiency is the number of statistical independent positions assured during blade rotation. The way to compute this quantity is still under investigation especially because its evaluation in a single chamber point does not give sufficient information about spatial correlation [38].

The common definition of stirrer independence is based on the evaluation of the (auto) correlation function. Even though it brings a simple and effective criterion, this perspective is still incomplete in evaluating whether a member of the cavity ensemble is strictly "independent" or not, with respect to the other realizations. Moreover, in using a RC a certain working volume (WV) is generally adopted to locate the device under test. It would be more reliable to evaluate the stirrer efficiency in terms of independent positions but analyzing the field correlation within the entire WV.

In this paper, we support the view of the reverberation chamber (RC) as a multivariate random field generator [39]. The effect of residual correlation has been proven to have an impact in goodness of fit tests [20]. Here, we discuss an alternative way of evaluating the number of independent positions of mechanical mode-stirrers. In particular, the proposed approach is based on the calculation of the correlation matrix for the magnitude of the electric field computed by FDTD code in a grid of N_w spatial points, selected among an arbitrary volume of the chamber. Another recent application of the correlation matrix to evaluated stirrer efficiency was applied to RC measurements based on a single point, adopting different frequency points to populate the matrix and investigating different chamber loading conditions [36].

2. REVERBERATION CHAMBER SETUP

Figure 1 shows the RC geometry used for both simulations and measurements: dimensions are $6.00 \times 4.00 \times 2.50\,\text{m}^3$. The fundamental mode resonance frequency is $f_0 = 45.04\,\text{MHz}$.

Two stirrers were placed along the y-axis (paddle shape) and the z-axis (Z-folded shape), and the investigated volume is between the two stirrers 0.5 m far from all metallic objects. The corner C of the investigated volume has the coordinates $(2.5, 1.0, 0.5)$ (m), and its dimension are $1.0 \times 2.0 \times 1.5\,\text{m}^3$. The vertical stirrer has a Z-folded shape, with a width of 1.2 m and a height of 2.4 m. The horizontal stirrer originally consisted of four $1\,\text{m} \times 0.5\,\text{m}$ separated panels subsequently joined by means of aluminum sheets to improve its performance. The mechanical engine, associated to each stirrer axis, allows to move them separately and in both stirring and stepped modes with a resolution of $1°$. The transmitting and receiving antennas are log-periodic operating between 300 MHz and 5 GHz (Schwarzbeck model USLP 9143). A VNA (Agilent E5071) was used to acquire the S_{21} parameter between the two antennas setting the maximum frequency resolution: 1601 points in each investigated sub-range. The VNA was calibrated adopting the standard procedure for transmission measurements, in order to account for all connecting cables: residual uncertainty is less than $\pm 0.2\,\text{dB}$ and $\pm 1°$. The data were acquired in tuned mode, moving the stirrers together, adopting synchronous and interleaved mode. When horizontal and vertical stirrers operate synchronously, they move with a step of $1°$ ($0° - 0°$, $1° - 1°$, $2° - 2°$, ..., $359° - 359°$) for a total of 360 positions. When they operate in interleaved mode, they move with a step of $19°$ each ($0° - 0°$, $0° - 19°$,
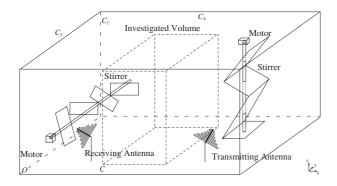

Figure 1. Chamber, stirrers and working volume. The dimensions of the chamber are $C_x = 6.00\,\text{m}$, $C_y = 4.00\,\text{m}$, and $C_z = 2.50\,\text{m}$.

$0° − 38°$, …, $19° − 0°$, $19° − 19°$, $19° − 38°$, …, $38° − 0°$, $38° − 19°$, $38° − 38°$, …, $342° − 0°$, $342° − 19°$, $342° − 38°$, …, $342° − 304°$, $342° − 323°$, $342° − 342°$), for a total of 361 positions [35].

3. FDTD FORMULATION

When a pulse is excited inside an RC, it will disappear only after a long time due to the high quality factor. The losses must be accounted in the simulations because they save computer resources and produce accurate results.

Our FDTD code has been extended and optimized to simulate the whole RC. The influence of wall losses on the equilibrium conditions was investigated for a the whole RC [26]. The same reference shows that it is possible to introduce artificial losses in the RC volume by neglecting the losses on the wall slightly affecting the field distributions. This approximation saves computer resources for a single FDTD simulation, in particular when a parallel computer is used. Moreover, when the statistical properties of the RC are simulated, the simulations must be repeated for each position of the stirrer. As consequence, the analysis of an RC when the stirrer is rotating requires multiple runs of FDTD code changing the angle of the stirrer. Each run is independent of the others, making it a "embarrassingly parallel" problem. Each FDTD simulation runs separately in a CPU of a high performance parallel computer, even without any parallelism of the code.

Usually, simulations of RC are helpful to investigate the frequencies up to about five time the lowest usable frequency (LUF). For the other frequencies, the required performance can be obtained with low design efforts. Under this assumption, the single simulation does not require a big computational effort, and can easily run on a single CPU of the parallel computer, because of the FDTD grid cell size depends on the working frequency.

Our RC was sampled in $201 × 134 × 84$ cubic cells with side $30\,\text{mm}$, the time step is $\Delta t = 50\,\text{ps}$, and the number of iteration is 206748. According to [26], we simulated ideal walls and we introduced some losses in the air. Comparing the measured and simulated decay factor of the RC with aluminum walls the air conductivity of $\sigma = 10^{-5}\,\text{S/m}$ gives the same results. Under this choice, the code is a standard FDTD code for any cell except for the two cells where the transmitting and receiving logperiodic antennas are fed. For those two points, an auxiliary line is connected to the antenna as described in [40]. The computer used for the simulations was an IBM P575 Power 6, with 5376 cores and 168 nodes. Each simulation for a stirrer position requires less than $500\,\text{MB}$ and less than 20 hours of CPU.

The numerical simulation uncertainty was evaluated using a power balance [26]. In the present case it is less than 3% because the ratio between the lowest wavelength and the cell size is about 14.

4. CORRELATION BY MULTIVARIATE ANALYSIS

We work out a method for evaluating the number of independent positions based on the statistical analysis of multiple fluctuating variables, namely multivariate analysis, collected inside the WV of a reverberation chamber. The simulation of the chamber of Fig. 1 allows for tracing the random field evolution inside the overall WV. In particular, we established a sampling grid of N_w points, each adjacent pair being equally-spaced of $\Delta x = 0.167\,\text{m}$, $\Delta y = 0.333\,\text{m}$, $\Delta z = 0.250\,\text{m}$, in the WV of Fig. 1. For any position of the stirrer and in the whole frequency range we have calculated, and stored, the three Cartesian components of the electromagnetic field in the $N_w = 7 \times 7 \times 7$ points of the WV.

5. MULTIDIMENSIONAL REVERBERATION

The mode-stirred chamber can be now characterized as a multidimensional random variable. Focusing on the total electric field, we define *multidimensional reverberation* $\underline{E}$ a collection

$$\{\underline{E}^{(\tau)} : \tau \in T\} \tag{1}$$

of R-valued multidimensional random variables $\underline{E}^{(\tau)} = \{E^{(m_i, m_j, m_k)}(\tau)\}$, in the probability space $\{\Omega, \underline{\mathcal{E}}, P\}$, where τ is the continuous stirring time instant, the local field $E^{(m_i, m_j, m_k)}(\tau)$ is picked up at the point $(m_i \Delta x, m_j \Delta y, m_k \Delta z)$ of the sampling grid made of N_w (spatial) sampling points, for each stir state $\tau_i = i\Delta\theta$, $i = 1, \ldots, N_s$, with $\Delta\theta$ angular stirrer step, N_s total number of stirrer positions considered in the analysis, and T total stirring length. The correlation is evaluated using N_p field values. In the case of the total electric field it is $N_p = N_w$, whereas for the three separate Cartesian components it is $N_p = 3N_w$.

The number of independent positions are evaluated dividing the number of elements of the correlation matrix, that is N_s^2, by the number of elements greater than the cutoff value of (11).

In this fashion, random variables and observations are organized

as follows

$$
\underline{\underline{e}} =
\begin{bmatrix}
e_1^{(1)} & e_1^{(2)} & \dots & e_1^{(N_s)} \\
e_2^{(1)} & e_2^{(2)} & \dots & e_2^{(N_s)} \\
e_3^{(1)} & e_3^{(2)} & \dots & e_3^{(N_s)} \\
\vdots & \vdots & \ddots & \vdots \\
e_{N_p}^{(1)} & e_{N_p}^{(2)} & \dots & e_{N_p}^{(N_s)}
\end{bmatrix}
=
\begin{bmatrix} \underline{e}^{(1)} & \underline{e}^{(2)} & \dots & \underline{e}^{(N_s)} \end{bmatrix},
\qquad (2)
$$

where thus the columns are random vectors made of fields at grid points, and the rows are (chamber) realizations made of stir states.

With reference to Section 6, the correlation can be evaluated in the frequency domain using two sets of the fields simulated for $N_s = 360$ stirrer locations.

By introducing a spatial grid, we implicitly account for the residual correlation between spatial points in calculating the correlation between stir states. As a matter of fact, the coarser the grid, and the higher the chamber operation frequency, the smaller the residual correlation. However, it is to be remarked that, because of the damped behavior of the spatial correlation function, its value is likely small and different from zero for most of the adjacent and non-adjacent points, but for those distances and excitation frequencies for which $n\lambda/2$. Therefore, we expect almost all small but not-null correlations for pair of points in the sampling lattice. It is thus quite natural to invoke the concept of a correlation matrix for analyzing the fluctuations in a multivariate stirring. This develops well on the use of the autocorrelation function [1], and of a two-point correlation function [38], widely used in RC analysis so far.

At low frequencies, many elements in such structured correlation matrix will be well above the uncorrelation limit (11), thus reducing its total number of eigenvalues, i.e., of principal components.

5.1. Correlation Matrix

The multidimensional reverberation can be efficiently used to overcome the drawbacks of the local reverberation point of view, such as the physical incompleteness of the single point autocorrelation in detecting unstirred components by goodness-of-fit tests. Here, the reasoning is driven by the multivariate analysis to explore the influence of a residual spatial correlation on the determination of the number of independent positions (N_{ind}).

Among the other possible ways of estimating N_{ind}, we propose a procedure based on the correlation matrix $\underline{\underline{R}}_{N_s \times N_s}$, calculated for all the possible pair combinations in the sampling grid, within $\{\tau_i\}$ stirrer

positions. In particular, for the single pair of spatial points, we use the correlation coefficient between two random vectors $\underline{e}_j$ and $\underline{e}_k$, modeling two random (Cartesian, total) fields collected in the FDTD sampling grid at two different stirrer positions j, and k. The Pearson definition of the correlation coefficient is usually employed in multivariate statistics, viz.,

$$\rho_{jk} = \frac{\mathrm{Cov}\left(\underline{e}^{(j)}, \underline{e}^{(k)}\right)}{\sqrt{\mathrm{Var}\left(\underline{e}^{(j)}\right)\mathrm{Var}\left(\underline{e}^{(k)}\right)}} = \frac{\sigma_{jk}}{\sqrt{\sigma_{jj}\sigma_{kk}}}, \qquad (3)$$

where $\mathrm{Cov}(\cdot, \cdot)$ stands for the covariance, $\mathrm{Var}(\cdot)$ stands for the individual field variance, and σ_{jk} has the meaning of an entry of the dispersion of the variance/covariance matrix of the field

$$\underline{\underline{\Sigma}} = \begin{bmatrix} \sigma_{11} & \sigma_{12} & \cdots & \sigma_{1N_s} \\ \sigma_{21} & \sigma_{22} & \cdots & \sigma_{2N_s} \\ \sigma_{31} & \sigma_{32} & \cdots & \sigma_{3N_s} \\ \vdots & \vdots & \ddots & \vdots \\ \sigma_{N_s 1} & \sigma_{N_s 2} & \cdots & \sigma_{N_s N_s} \end{bmatrix}, \qquad (4)$$

where thus

$$\underline{\underline{\Sigma}} = \mathrm{E}\left[\left(\underline{\underline{e}} - \underline{\underline{\mu}}_e\right)^T \left(\underline{\underline{e}} - \underline{\underline{\mu}}_e\right)\right] = \mathrm{E}\left[\underline{\underline{e}}^T \underline{\underline{e}}\right] - \underline{\underline{\mu}}_e^T \underline{\underline{\mu}}_e, \qquad (5)$$

with $(\cdot)^T$ representing the matrix transpose, $\underline{\underline{e}}$ defined as in (2), and N_s the number of stirrer positions being considered in the evaluation of independence, thus obtained discretizing the time-domain stirring process as depicted in (2). It is worth remarking that it is expected to have many dependent pairs within N_s, so typically $N_{ind} \leq N_s$. For the sake of completeness, we remind that the quantity $\mathrm{Tr}\left[\underline{\underline{\Sigma}}\right] = \sum_{i=1}^{N_s} \sigma_{ii} = \hat{\sigma}$ is called the total variance, and the determinant of $\underline{\underline{\Sigma}}$, denoted by $\left|\underline{\underline{\Sigma}}\right|$, is referred as the generalized variance. Accordingly, we define the correlation matrix of $\underline{e}$ as

$$\underline{\underline{R}} = \begin{bmatrix} \rho_{11} & \rho_{12} & \cdots & \rho_{1N_s} \\ \rho_{21} & \rho_{22} & \cdots & \rho_{2N_s} \\ \rho_{31} & \rho_{32} & \cdots & \rho_{3N_s} \\ \vdots & \vdots & \ddots & \vdots \\ \rho_{N_s 1} & \rho_{N_s 2} & \cdots & \rho_{N_s N_s} \end{bmatrix} = \left[\mathrm{Tr}\left(\underline{\underline{\Sigma}}\right)\right]^{-1/2} \underline{\underline{\Sigma}} \left[\mathrm{Tr}\left(\underline{\underline{\Sigma}}\right)\right]^{-1/2}. \qquad (6)$$

At this point, the multivariate point of view comes into play: having collected a large amount of data points from FDTD simulations, we can estimate the spatial average $\underline{\underline{\mu}}_e$. This is actually calculated among the chamber volume covered by the FDTD sampling lattice, thus tracing for the field fluctuation through a reverberation sub-volume established by the mode-stirrer effectiveness.

5.2. Correlation Coefficient among Space Lattices

The multivariate perspective we adopted throughout the paper gives a unified picture of the chamber statistics. Focusing on the Pearson correlation coefficient, we remark it is subject to statistical uncertainty and fluctuations driven by statistical moments of underlying data. This effect can be readily understood and quantified thanks to the Fisher theory on correlation distribution [41]. In the late '40, Fisher has been able to derive closed-form solutions for the distribution of $r = \rho_{jk}$ by exploiting a geometrical perspective of the Pearson expression. Its expression, assuming as $\underline{e}^{(j)}$ the vector collecting N_p realizations of the j-th i.i.d. zero mean Gaussian variable, among the N_s ones, reads [41]

$$f_M\left(r, \overline{r}\right) = \frac{(M-2)\,\Gamma\left(M-1\right)\left(1 - \underline{r}^2\right)^{\frac{M-1}{2}}\left(1 - r^2\right)^{\frac{M-4}{2}}}{\sqrt{(2\pi)}\Gamma\left(M - \frac{1}{2}\right)\left(1 - \underline{r}r\right)^{M-\frac{3}{2}}}$$
$$\times F_G\left[\frac{1}{2}, \frac{1}{2}; \frac{2M-1}{2}, \frac{\underline{r}r + 1}{2}\right],\qquad(7)$$

where M is the number of *uncorrelated* samples, and F_G is the Gaussian hypergeometric function.

The correlation distribution has been originally used in evaluating the significance of the autocorrelation values in local RC measurements [42]. Actually, once specified the uncorrelation bound $\underline{r}$, e.g., $\underline{r} = 0$, or $\underline{r} = 1/e$, the Fisher distribution (7) indicates that even highly deviated value of correlation can occur with finite probability thus calling for a more precise, and yet physical based, definition of *independence* given a certain amount of *uncorrelation*.

Beside this, we should also point out that in a multivariate perspective based on lattices, ρ_{jk} depends on the autocorrelation between (spatial) points used to estimate the second-order statistics. The present study constitutes a starting point towards the definition of independency accounting for all the effects we mentioned so far, i.e., statistical inhomogeneity and anisotropy captured by the multivariate (lattice) perception for each stirrer location, spatial autocorrelation introduced by the sampling grid, and fluctuation of the Pearson correlation due to its pure mathematical definition. However, the results we will show in the next section account for all of this through the numerical estimation of the uncorrelated positions.

6. EVALUATION OF STIRRER UNCORRELATED POSITIONS

A result of the measurements and of the simulations is the S_{21} parameter. Over a stirrer rotation, N received sampled data are

acquired and stored in an array a. It is periodic with period N ($a_i = a_{i+kN}$ with $k \in \mathbb{Z}$). Following the standard [1], the i-value of the autocorrelation array is computed as

$$\rho_i = \frac{\sum_{j=0}^{N-1} (a_j - \langle a \rangle)(a_{j+i} - \langle a \rangle)}{(N-1)\,\sigma_{2a}}, \tag{8}$$

where $0 \leq i \leq N - 1$, and

$$\sigma_{2a} = \frac{1}{N-1} \sum_{j=0}^{N-1} (a_j - \langle a \rangle)^2 \tag{9}$$

is the variance of the array a.

We introduce a new criterion for estimating the number of independent stirrer configurations. This is useful to evaluate the effectiveness of different stirrer geometries against working frequencies RC is operated at. A rather natural extension of the normative procedure, based on the autocorrelation function [1], might rely on the correlation matrix (6). One is indeed tempted to say that two stirrer configurations are uncorrelated if and only if $\rho_{jk} < 1/e$. The number of elements satisfying this condition can thus be treated as the number of uncorrelated positions N_{ind} produced by the stirring procedure. Obviously, we should account for the symmetry properties of (6), thus excluding redundant elements yields

$$N_{ind} = \frac{\#\left[\underline{\underline{R}} < r\underline{\underline{1}}\right]}{2}, \tag{10}$$

where $\#\left[\cdot\right]$ is the counting operator, $\underline{\underline{1}}$ is the identity matrix of dimension N_s, and r is the cutoff value set following the new release of standard [1] to

$$r = \frac{1}{e}\left[1 - \frac{7.22}{(N_s^2)^{0.64}}\right]. \tag{11}$$

When two stirrers are used in an RC, we follow the procedure described in [35].

7. RESULTS

In this section the number of independent positions computed by multivariate analysis correlation (MAC) is compared to that obtained by the classical circular correlation (CC) adopted for both numerical and experimental data [1]. The comparison is done for both stirrer

moving modes. Moreover, the effects on the MAC results varying the
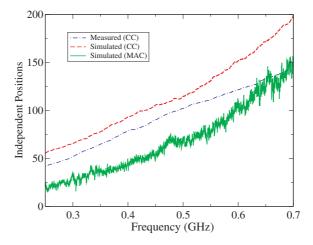total number of the spatial points and their relative distance are also
investigated.

Figure 2. Number of independent positions computed by measured
and simulated data when the stirrers move in synchronous mode. They
are compared with those obtained using the correlations, evaluated
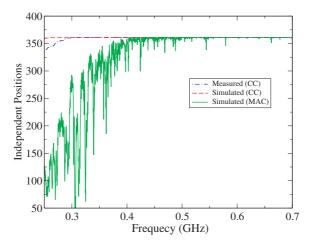over the magnitude of the electric field.

Figure 3. Number of independent positions computed by measured
and simulated data when the stirrers move in interleaved mode. They
are compared with those obtained using the correlations, evaluated
over the magnitude of the electric field.

The results obtained by the MAC method are shown in Figs. 2 and 3 for synchronous and interleaved mode respectively. Of course the interleaved mode ensures a higher number of independent positions, that reaches the maximum explored value of 360 around 450 MHz. The two figures also reports what obtained applying the CC method, both numerically and experimentally. The traditional CC method overestimates the independent position number and this is the main reason why we introduce the MAC method. This behavior of the CC results was also observed in the past, for the same chamber and the same stirrer configurations, analyzing the ratio between the maximum and the ensemble averaged field inside the chamber whose value is related, in a statistical sense, to the independent position number [35]. Similar results were observed in [36] with a different work methodology and higher frequency range.

Figure 4 shows the effect produced by the number of field points used to build up the correlation matrix. In particular, the same total volume is considered, but the grid varies from a $7 \times 7 \times 7 = 343$ to a $3 \times 3 \times 3 = 27$ points. When the three Cartesian field components are taken for each point, the correlation is computed over a set three times larger.

The figure refers to the interleaved mode case, because the higher independent position number allows us to better highlight the effect of each variation in the spatial point number used for the correlation matrix. The MAC method exhibits an asymptotic behavior when the
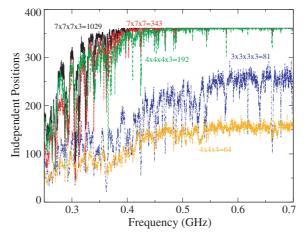

Figure 4. Simulated number of independent positions in the interleaved mode. The spatial points are varied from a grid of $7 \times 7 \times 7$ to a grid of $3 \times 3 \times 3$ points. The correlation matrix was build up using the total electric field, or the three separate Cartesian components.

field point number increases. More precisely, the 343 values obtaining
adopting the total electric field values already give good results that
can be improved very little if the three separate rectangular field
components are employed, so reaching 1029 values. On the contrary,
adopting a $4 \times 4 \times 4$ grid, that gives only 64 values for the total
electric field, the MAC results is visible bad. If we consider all the
field rectangular components for this last grid, reaching 192 values,
the computed independent positions are similar to those obtained by
the previous densest grid. This direct link to the total field samples
used is further confirmed if we consider a less dense grid, $3 \times 3 \times 3$,
but with all field components for a total of 81 values: the result is
better than the $4 \times 4 \times 4$ case with only the total field. The previous
analysis was carried out assuming the same volume for the grid, so
increasing the distance between each spatial point when the grid was
less dense. Which is the optimal distance to be taken? The issue
of the distance capable to assure spatial uncorrelation was intensively
addressed in literature [38, 43], leading to suggest a distance of about
one half of wavelength. To investigate this aspect for the MAC method
let's consider the results reported in Fig. 5. It compares the MAC
computed independent positions for the same spatial point number
$4 \times 4 \times 4$ previously shown in Fig. 4 (large volume), and for a lower
point distance (reduced volume).

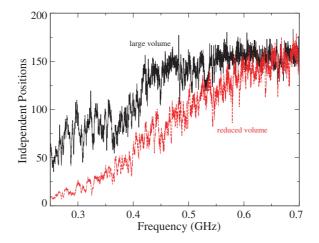It can be noted that the reduced volume gives the same results

Figure 5. Simulated number of independent positions in the
interleaved mode. The spatial points distance is halved from that of
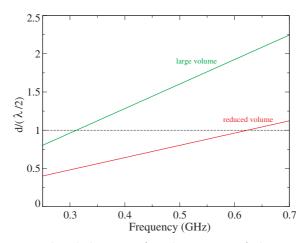Fig. 4 (large volume) maintaining the same total number of points.

Figure 6. Normalized distance for the points of the two volumes of Fig. 5.

of the larger one for frequencies above 600 MHz. The explanation can be found in analyzing the point distance in terms of wavelength at the operating frequencies. More precisely, Fig. 6 reports this point distance normalized to half wavelength for both grids. Because the WV is not a cube, the distance between each point is not uniform along the three Cartesian coordinates. Therefore, Fig. 6 considers an equivalent volume cube side ($d = \sqrt[3]{\Delta x \Delta y \Delta z}$), because it represents a sort of averaged distance between two adjacent points of the grid. It can be clearly seen that this averaged distance becomes compared to a half of wavelength around 600 MHz, where the results obtained by the reduced volume overlap to those of the larger one.

8. CONCLUSIONS

The uncorrelated positions of two stirrers have been computed by means of the correlations method of multiple spatial points in an RC. Two kinds of moving mode for the two stirrers were investigated: synchronous and interleaved. In both cases we showed that the traditional way based on the CC overestimates the uncorrelated position number. The larger is the volume adopted to calculate the correlation matrix, the more reliable is the obtained values. Moreover, the importance of the correlation distance between two adjacent points of the spatial grid has been investigated.

The proposed method is based on the knowledge of field values in a grid of points inside the chamber WV. This can be time consuming

for investigation of an existing chamber. On the other hand, it can be easily adopted during the design by numerical simulation of a new chamber and new stirrers.

ACKNOWLEDGMENT

REFERENCES

1. International Standards-IEC 61000-4-21, "Electromagnetic compatibility (EMC) — Part 4-21: Testing and measurement techniques — Reverberation chamber test methods," 2.0 Ed., Geneva, Switzerland, 2011.

2. Mariani Primiani, V. and F. Moglie, "Numerical simulation of LOS and NLOS conditions for an antenna inside a reverberation chamber," *Journal of Electromagnetic Waves and Applications*, Vol. 24, Nos. 17–18, 2319–2331, 2010.

3. Chen, X., "Measurements and evaluations of multi-element antennas based on limited channel samples in a reverberation chamber," *Progress In Electromagnetics Research*, Vol. 131, 45–62, 2012.

4. Pomianek, A. J., K. Staniec, and Z. Joskiewicz, "Practical remarks on measurement and simulation methods to emulate the wireless channel in the reverberation chamber," *Progress In Electromagnetics Research*, Vol. 105, 49–69, 2010.

5. Staniec, K. and A. J. Pomianek, "On simulating the radio signal propagation in the reverberation chamber with the ray launching method," *Progress In Electromagnetics Research B*, Vol. 27, 83–99, 2011.

6. Genender, E., C. L. Holloway, K. A. Remley, J. M. Ladbury, G. Koepke, and H. Garbe, "Simulating the multipath channel with a reverberation chamber: Application to bit error rate measurements," *IEEE Transactions on Electromagnetic Compatibility*, Vol. 52, No. 4, 766–777, 2010.

7. Centeno, A. and N. Alford, "Measurement of zigbee wireless communications in mode-stirred and mode-tuned reverberation chamber," *Progress In Electromagnetics Research M*, Vol. 18, 171–178, 2011.

8. Staniec, K., "Evaluation of the zigbee transmission repetition

mechanism in the variably-loaded reverberation chamber," *Progress In Electromagnetics Research*, Vol. 132, 297–314, 2012.

9. El Baba, I., S. Lalléchère, and P. Bonnet, "Numerical total scattering cross section from reverberating electromagnetic experiments," *Progress In Electromagnetics Research Letters*, Vol. 19, 127–135, 2010.

10. Lalléchère, S., S. Girard, D. Roux, P. Bonnet, F. Paladian, and A. Vian, "Mode stirred reverberation chamber (MSRC): A large and efficient tool to lead high frequency bioelectromagnetic in vitro experimentation," *Progress In Electromagnetics Research B*, Vol. 26, 257–290, 2010.

11. Moglie, F., V. Mariani Primiani, and A. P. Pastore, "Modeling of the human exposure inside a random plane wave field," *Progress In Electromagnetics Research B*, Vol. 29, 251–267, 2011.

12. Gradoni, G., F. Moglie, A. P. Pastore, and V. Mariani Primiani, "Numerical and experimental analysis of the field to enclosure coupling in reverberation chamber and comparison with anechoic chamber," *IEEE Transactions on Electromagnetic Compatibility*, Vol. 48, No. 1, 203–211, 2006.

13. Fedeli, D., G. Gradoni, V. Mariani Primiani, and F. Moglie, "Accurate analysis of reverberation field penetration into an equipment-level enclosure," *IEEE Transactions on Electromagnetic Compatibility*, Vol. 51, No. 2, 170–180, 2009.

14. Mariani Primiani, V., F. Moglie, and A. P. Pastore, "Field penetration through a wire mesh screen excited by a reverberation chamber field: FDTD analysis and experiments," *IEEE Transactions on Electromagnetic Compatibility*, Vol. 51, No. 4, 883–891, 2009.

15. Wang, Q., E. Cheng, and Z. Qu, "On the shielding effectiveness of small-dimension enclosures using a reverberation chamber," *IEEE Transactions on Electromagnetic Compatibility*, Vol. 53, No. 3, 562–569, 2011.

16. Lampasi, D. A. and M. S. Sarto, "Shielding effectiveness of a thick multilayered panel in a reverberating environment," *IEEE Transactions on Electromagnetic Compatibility*, Vol. 53, No. 3, 579–588, 2011.

17. Moglie, F., D. Micheli, S. Laurenzi, M. Marchetti, and V. Mariani Primiani, "Electromagnetic shielding performance of carbon foams," *Carbon*, Vol. 50, No. 5, 1972–1980, 2012.

18. Holloway, C. L., D. A. Hill, J. Ladbury, G. Koepke, and R. Garzia, "Shielding effectiveness measurements of materials using nested reverberation chambers," *IEEE Transactions on Electromagnetic*

Compatibility, Vol. 45, No. 2, 350–356, 2003.

19. Hill, D. A., "Electronic mode stirring for reverberating chambers," *IEEE Transactions on Electromagnetic Compatibility*, Vol. 36, 294–299, 1994.

20. Cozza, A., "The role of losses in the definition of the overmoded condition for reverberation chambers and their statistics," *IEEE Transactions on Electromagnetic Compatibility*, Vol. 53, No. 2, 296–307, 2011.

21. Serra, R. and F. G. Canavero, "Bivariate statistical approach for 'good-but-imperfect' electromagnetic reverberation," *IEEE Transactions on Electromagnetic Compatibility*, Vol. 53, No. 3, 554–561, 2011.

22. Gradoni, G. and L. R. Arnaut, "Generalized extreme-value distributions of power near a boundary inside electromagnetic reverberation chambers," *IEEE Transactions on Electromagnetic Compatibility*, Vol. 52, No. 3, 506–515, 2010.

23. Vaccari, A., A. Cala'Lesina, L. Cristoforetti, and R. Pontalti, "Parallel implementation of a 3D subgridding FDTD algorithm for large simulations," *Progress In Electromagnetics Research*, Vol. 120, 263–292, 2011.

24. Edwards, R., A. Marvin, and S. Porter, "Uncertainty analyses in the finite-difference time-domain method," *IEEE Transactions on Electromagnetic Compatibility*, Vol. 52, No. 1, 155–163, 2010.

25. Mengue, S., E. Richalot, and O. Picon, "Comparison between different criteria for evaluating reverberation chamber functioning using a 3-D FDTD algorithm," *IEEE Transactions on Electromagnetic Compatibility*, Vol. 50, No. 2, 237–245, 2008.

26. Moglie, F., "Convergence of the reverberation chambers to the equilibrium analyzed with the finite-difference time-domain algorithm," *IEEE Transactions on Electromagnetic Compatibility*, Vol. 46, No. 3, 469–476, 2004.

27. Amador, E., C. Lemoine, P. Besnier, and A. Laisné, "Reverberation chamber modeling based on image theory: Investigation in the pulse regime," *IEEE Transactions on Electromagnetic Compatibility*, Vol. 52, No. 4, 778–789, 2010.

28. Zhao, H. and Z. Shen, "Hybrid discrete singular convolution-nmethod of moments analysis of a 2-d transverse magnetic reverberation chamber," *IEEE Transactions on Electromagnetic Compatibility*, Vol. 52, No. 3, 612–619, 2010.

29. Moglie, F. and A. P. Pastore, "FDTD analysis of plane waves superposition to simulate susceptibility tests in reverberation

chambers," *IEEE Transactions on Electromagnetic Compatibility*, Vol. 48, No. 1, 195–202, 2006.

30. Magdowski, M., S. V. Tkachenko, and R. Vick, "Coupling of stochastic electromagnetic fields to a transmission line in a reverberation chamber," *IEEE Transactions on Electromagnetic Compatibility*, Vol. 53, No. 2, 308–317, 2011.

31. West, J. C., C. F. Bunting, and V. Rajamani, "Accurate and efficient numerical simulation of the random environment within an ideal reverberation chamber," *IEEE Transactions on Electromagnetic Compatibility*, Vol. 54, 2012.

32. Mariani Primiani, V. and F. Moglie, "Numerical simulation of reverberation chamber parameters affecting the received power statistics," *IEEE Transactions on Electromagnetic Compatibility*, Vol. 54, No. 3, 522–532, 2012.

33. Nisanci, M., E. Küüksille, Y. Cengiz, A. Orlandi, and A. Duffy, "The prediction of the electric field level in the reverberation chamber depending on position of stirrer," *Expert Systems with Applications*, Vol. 38, No. 3, 1689–1696, 2011.

34. Hong, J.-I. and C.-S. Huh, "Optimization of stirrer with various parameters in reverberation chamber," *Progress In Electromagnetics Research*, Vol. 104, 15–30, 2010.

35. Moglie, F. and V. Mariani Primiani, "Analysis of the independent positions of reverberation chamber stirrers as a function of their operating conditions," *IEEE Transactions on Electromagnetic Compatibility*, Vol. 53, No. 2, 288–295, 2011.

36. Pirkl, R. J., K. A. Remley, and C. S. Lötbäck Patané, "Reverberation chamber measurement correlation," *IEEE Transactions on Electromagnetic Compatibility*, Vol. 54, No. 3, 533–545, 2012.

37. Moglie, F. and V. Mariani Primiani, "Numerical analysis of a new location for the working volume inside a reverberation chamber," *IEEE Transactions on Electromagnetic Compatibility*, Vol. 54, No. 2, 238–245, 2012.

38. Amador, E., C. Lemoine, and P. Besnier, "Numerical study of spatial correlation in reverberation chamber," *Electronics Letters*, Vol. 47, No. 24, 1319–1320, 2011.

39. Cozza, A., "A skeptic's view of unstirred components," *EMC Europe 2011*, 174–179, York, UK, Sep. 2011.

40. Maloney, J. G., K. L. Shlager, and J. S. Smith, "A simple FDTD model for transient excitation of antennas by transmission lines," *IEEE Trans. Antennas Propag.*, Vol. 42, No. 2, 289–292, 1994.

41. Anderson, T. W., "R. A. Fisher and multivariate analysis,"

Statistical Science, Vol. 11, No. 1, 20–34, 1996.

42. Wellander, N., O. Lunden, and M. Backstrom, "Experimental investigation and mathematical modeling of design parameters for efficient stirrers in mode-stirred reverberation chambers," *IEEE Transactions on Electromagnetic Compatibility*, Vol. 49, No. 1, 94–103, 2007.

43. Hill, D. A. and J. Ladbury, "Spatial-correlation functions of fields and energy density in a reverberation chamber," *IEEE Transactions on Electromagnetic Compatibility*, Vol. 44, No. 1, 95–101, 2002.